Study on Winding Method and Mechanical-electronic Design for High-speed Operation of Electric Motor

Jin-Uk Choi¹, Jae-Kwang Lee¹, Dong-Hoon Jung², Yang-Jin Shin³, Ju Lee³, and Ki-Doek Lee^{1*}

¹Intelligent Mechatronics Research Center, Korea Electronics Technology Institute, Gyeonggi-do 14502, Republic of Korea ²School of Advanced Materials and Electrical Engineering, GyeongKuk National University, Andong 36729, Republic of Korea ³Department of Electrical Engineering, Hanyang University, Seoul 04763, Republic of Korea

(Received 13 May 2025, Received in final form 22 June 2025, Accepted 23 June 2025)

In response to the tightening of environmental regulations due to climate change and the gradual depletion of fossil fuel resources, the automobile industry is accelerating the transition from conventional internal combustion engine systems to high-efficiency, low-carbon electric drive systems. This shift applies not only to passenger cars but also to high-performance vehicles such as sports cars. In high-performance electric vehicles that employ a fixed gear ratio, the drive motor's rotational speed is directly linked to the vehicle's wheel speed. Therefore, a high-speed motor design is essential to expand the vehicle's driving speed range. In this study, we conducted a detailed analysis of a commercial model from a leading manufacturer capable of operating at over 20,000 RPM to derive its input/output characteristics. Based on this analysis, we designed a drive motor capable of achieving even higher speeds under the same output conditions. The number of poles was selected to ensure sufficient control resolution within the limited switching frequency of the insulated-gate bipolar transistor (IGBT) elements during high-speed operation. Additionally, the optimal winding type for high-speed driving was determined by comparing the AC loss characteristics of hairpin windings with a round-wire model using parallel strands. To ensure mechanical reliability, the rotor design was optimized to reduce stress during high-speed operation. To validate the proposed motor design, efficiency maps were generated across the full driving range to assess output characteristics. Finally, a prototype was fabricated and tested to confirm the validity of the design.

Keywords: IPMSM, electric vehicles, traction motor, stator windings, high speed design

1. Introduction

The Climate Change Convention, which aimed to reduce and eliminate greenhouse gas emissions contributing to global warming, came into effect in March 1994. Since then, all member countries—categorized as developed and developing nations—have been making voluntary and coordinated efforts to reduce greenhouse gas emissions. Furthermore, following the crisis faced by global automaker W, automotive companies worldwide have been responding to fuel economy and emissions regulations by developing eco-friendly electric vehicles and green

cars that use environmentally friendly energy sources as alternatives to internal-combustion engines.

In line with these developments, the automotive industry has increasingly focused on creating vehicles powered solely by electric motors or by hybrid systems that combine electric motors with internal-combustion engines. Among the various types of vehicles, electric vehicles (EVs) are currently garnering significant attention. The electric motors used in EVs must meet demanding requirements, including a wide operating range, high power output, and high efficiency [1, 2].

Until a few years ago, electric vehicles were primarily limited to small- and medium-sized passenger cars due to limited driving performance and range. However, more recently, a broader variety of vehicles—including commercial vehicles and sports cars—have been electrified, driven by improvements in electric drive system performance and increased battery energy density [3]. Established high-performance vehicle manufacturers such

©The Korean Magnetics Society. All rights reserved.

*Corresponding author: Tel: +82-32-621-2869

e-mail: kdlee@keti.re.kr

This paper was presented at the IcAUMS 2025, Okinawa, Japan, April 21-24, 2025.

as Porsche, BMW, Mercedes-Benz, and Audi have also entered the EV market. Hyundai-Kia Motors, for instance, has introduced a model equipped with a 21,000-RPM drive motor as a high-performance vehicle. Other global companies, including Tesla (USA) and Rimac (Croatia), have developed and released high-performance EVs featuring top-tier speed and acceleration, supported by electric drive systems operating above 20,000 RPM.

Most modern high-performance battery electric vehicles (BEVs) utilize gear systems with fixed reduction ratios ranging from 7:1 to 10:1. Due to this configuration, the drive motor's torque is directly transmitted to the wheels, and its rotational speed is directly linked to the vehicle's wheel speed. When a high-speed drive motor is paired with a reducer using a currently mass-produced reduction ratio, the output speed after reduction increases. As a result, the vehicle can achieve maximum speed performance equal to or greater than that of a high-speed internalcombustion engine vehicle. Moreover, when combined with a reducer having a higher reduction ratio, the output speed can be maintained at the current level while significantly increasing the vehicle's wheel torque—the output of the reducer. This makes such configurations highly suitable for high-performance vehicles requiring high-torque characteristics, offering considerable advantages in terms of performance enhancement through the use of high-speed drive motors.

Recently, research has actively focused on using hairpin windings with high power density, achieved through a high slot-fill factor, as a method to enhance the performance of EV drive motors [4]. However, in mass-produced BEV drive motors employing hairpin windings, the maximum rotational speed typically remains below 20,000 RPM [5]. Since this paper addresses the design of a drive motor with a target rotational speed of 25,000 RPM, it is

important to consider the influence of AC copper losses occurring in hairpin windings at high speeds. Accordingly, the suitability of different winding types for high-speed applications must be evaluated, particularly by comparing hairpin windings with circular windings using parallel strands, which mitigate AC copper loss [6].

Additionally, if the stress generated in the rotor due to centrifugal forces during high-speed rotation exceeds the material's yield strength, permanent deformation or structural failure may occur. Therefore, it is essential to investigate rotor design strategies that reduce mechanical stress and ensure a sufficient safety factor at the target maximum speed [7, 8].

2. Analysis of Leading Industry Products

In this study, a commercially available model from leading company 'H', capable of operating above 20,000 RPM, was thoroughly analyzed, and a reverse-engineered model was developed based on the findings. The geometry and specifications of the reverse-engineered model are summarized in Fig. 1(a) and Table 1. Assuming a current density that accounts for the applied cooling method, the input and output characteristics were derived based on the number of conductors per slot and the slot geometry (e.g., area).

The analysis revealed that the stator winding employed a hairpin winding configuration, with six windings inserted per slot. For the stator, the analysis considered factors such as the cooling method, slot geometry, number of parallel circuits, and lamination stack. To estimate the net copper area of the hairpin winding, the thicknesses of the insulation coating and slot liner were assumed based on commercial product information. The coil shapes and specifications derived from the analysis are shown in Fig.

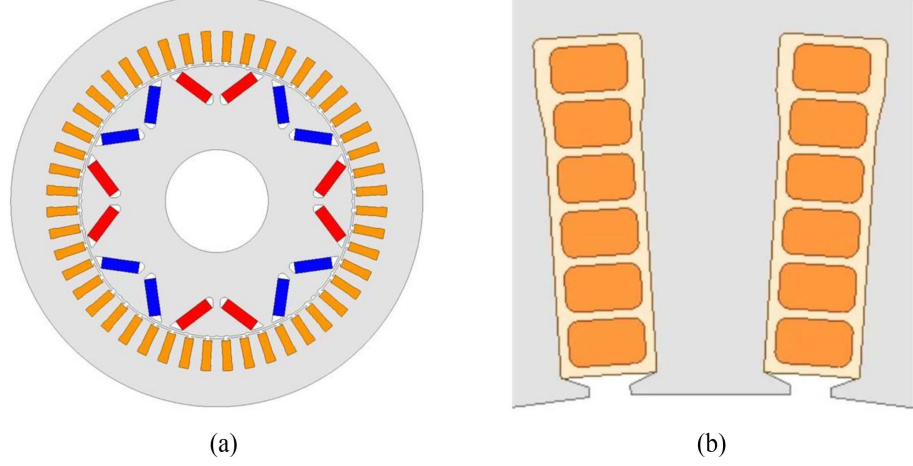


Fig. 1. (Color online) Shape of Commercial Model (a) Reverse-Engineered Model, (b) Stator Coil.

Table 1.	Analysis	Result	of (Commercial	Model.

It	em	Unit	Value	Remark
Motor Type		-	IPMSM	V Type Magnet
Poles	Poles / Slots		8P / 48S	
Battery	Voltage	V_{dc}	800	
Stator	Out Dia	mm	200	
Stator	Inner Dia	mm	133.6	
Rotor	Out Dia	mm	132	
KOIOI	Inner Dia	mm	50	
Stack	Length	mm	160	
Airgap	Length	mm	0.8	
Material	Steel	-	25PNF1250F	Estimated based on material geometry
iviateriai	Magnet	-	N48UH	and performance

Table 2. Analysis Result of Commercial Model Stator Windings.

Item		Unit	Value	Remark
Winding Type		-	Hairpin	
Num of Layer		-	6	
Cool	Cooling Method		Oil Cooling	
Currer	Current density (A)		25	
Paralle	Parallel circuits (B)		2	
	Width	mm	3.34	
Coil Size	Height	mm	2	
Area (C)		mm^2	6.68	Width * Height
Input current per Coil (D)		A_{rms}	167	D = A * C
Input current (E)		A_{rms}	334	E = B * D

1(b) and Table 2, respectively. As shown in Table 2, after excluding the insulation coating and slot liner within the slot area, a conductor with a width of 3.34 mm and height of 2 mm could be inserted. Based on the current density and number of parallel circuits, the motor input current was reverse calculated to confirm that a current of approximately 334 [Arms] could be applied.

For the electric motor, once the geometric parameters and voltage and current limits are defined, the motor's output characteristics can be derived. Based on the previous analysis, the battery voltage $(800V_{dc})$ and motor input current $(334A_{rms})$ were assumed as the voltage and current limits for this analysis.

Table 3 presents the motor's input/output characteristics at various operating points, excluding losses that cannot be determined through electromagnetic field analysis, such as mechanical losses and stray load losses. The maximum torque was found to be 330[Nm], and the maximum output reached 220[kW]. The analysis was conducted within the defined voltage limit, using the

fundamental component of the induced voltage, confirming that operation at 21,000 RPM is feasible.

However, in the high-speed range, a significant drop in efficiency was observed due to increased AC losses in the stator hairpin winding. Fig. 2(a) shows the N-T-P (speed-torque-power) curve under maximum-output control for the commercial model, while Fig. 2(b)

Table 3. Load Analysis Result for Commercial Model.

Item	Unit		Operating Point			
Item	Oiii	Max Eff	Max Output	Max Speed		
I_a	A_{rms}	100	334	310		
Current Phase Angle	deg	24	56	83		
Rotation Speed	r/min	5,100	6,300	21,000		
Torque	Nm	105	333	91		
Input Power	kW	58	236	228		
Output Power	kW	55.9	220	200		
Efficiency	%	95.7	93.4	87.7		

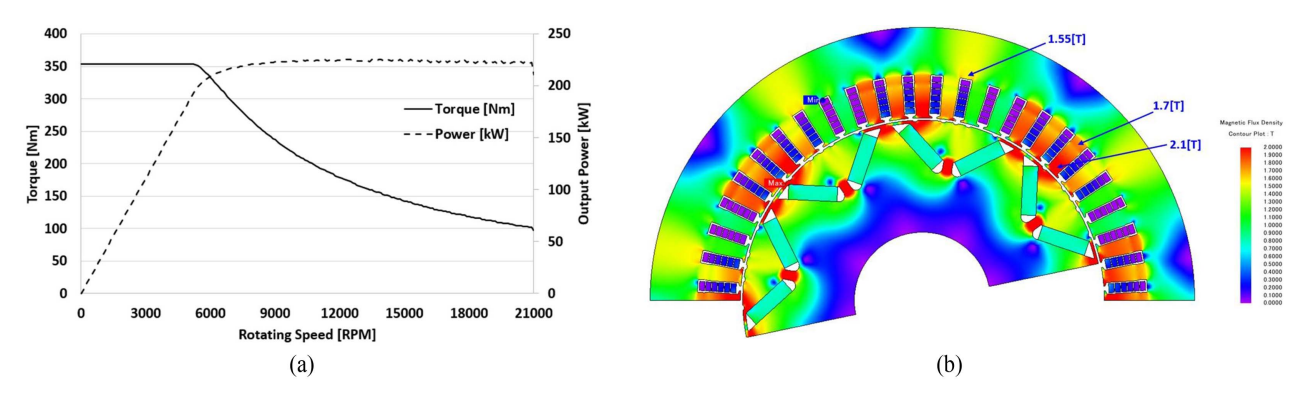


Fig. 2. (Color online) Input/Output characteristics of Commercial Model (a) N-T-P Curve, (b) Magnetic Flux Density distribution

illustrates the magnetic flux density distribution at the maximum-output operating point.

3. High-Speed Optimized Design for 25,000RPM Operation

3.1. Adjusting the Number of Poles to Ensure Switching Counts

The number of poles in the motor affects its size and controllability. As the number of poles increases, the magnetic-flux saturation of the stator yoke decreases, which reduces the size of the motor. However, as the operating frequency increases, controllability deteriorates; therefore, the control frequency and operating speed must be considered when selecting the number of poles [9]. As shown in Table 4, assuming the switching frequency is 16

[kHz] and driving the motor at a speed of 25,000 RPM, it can be seen that the number of poles must be selected to 6 or less to secure more than 10 sampling counts within one cycle of the switching frequency [10].

3.2. Review of Winding Types Suitable for High-Speed Operation

The stator winding method was selected based on the motor's cooling method, load point, and application system. In general, round-wire windings are used in industrial and household appliances, while hairpin windings are applied in high-power, high-performance motors. Fig. 3 illustrates the shapes and conceptual diagrams of both winding methods.

Round-wire winding, commonly used in industrial, household, and automotive applications, offers advantages

Table 4. Calculating Switching Counts by Pole Number.

Item	Unit	Case1	Case2	Case3	Case4	
Switching Frequency	Hz	16,000				
Rotation Speed	r/min		25,0	000		
Poles	-	4	6	8	10	
Electrical Frequency	Hz	833	1250	1667	2083	
Sampling Counts (per Cycle)	-	19.2	12.8	9.6	7.7	

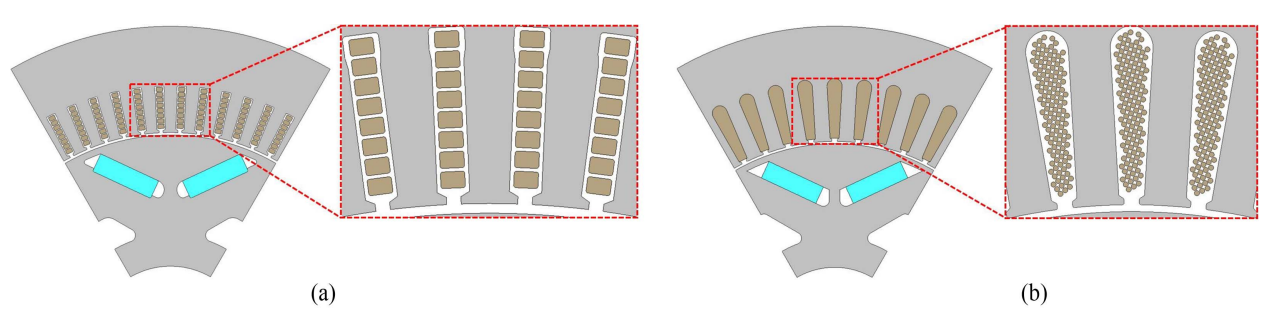


Fig. 3. (Color online) Design Model Shapes by winding type (a) Hairpin Coil, (b) Round Wire (using parallel strands).

in terms of design flexibility and manufacturability by implementing stator windings using parallel strands. Moreover, since the wire area exposed to the magnetic flux during motor operation is relatively small, the AC copper loss—including eddy current loss caused by flux variation—is reduced. This gives round-wire windings an efficiency advantage in high-speed operation. However, a major drawback is their lower space factor, which is reduced by more than 20% compared to hairpin windings, potentially limiting power density [11].

Hairpin winding, on the other hand, offers a high slot-fill factor exceeding 60%, making it well-suited for high-power-density motors and significantly enhancing power density compared to round-wire windings. However, since the number of series turns is constrained by the number of coil layers and slots, hairpin winding designs face certain limitations. Additionally, hairpin winding is more difficult to manufacture, and the initial investment cost for mass production is high. Another disadvantage is that the larger conductor area exposed to magnetic flux

increases AC losses during high-speed operation, resulting in lower efficiency.

The commercial model analyzed in Chapter 2 employed a hairpin winding structure. However, as the target maximum operating speed increased, two types of winding models were designed—considering the influence of AC copper loss—in order to derive the input and output characteristics across the entire operating range.

Both models were designed under the same electric (same number of turns and current density) and magnetic loading conditions. In the hairpin winding model, because of the higher slot-fill factor, a smaller slot area was sufficient to achieve the same electric loading. As shown in Fig. 4, the hairpin winding model has a generous tooth width of the stator iron core; therefore, the magnetic saturation is lowered, and iron loss is reduced. However, as the operating speed increased, the AC copper loss of the hairpin winding increased significantly, causing a sharp reduction in the output power and efficiency. However, in the round-wire winding model, a larger slot

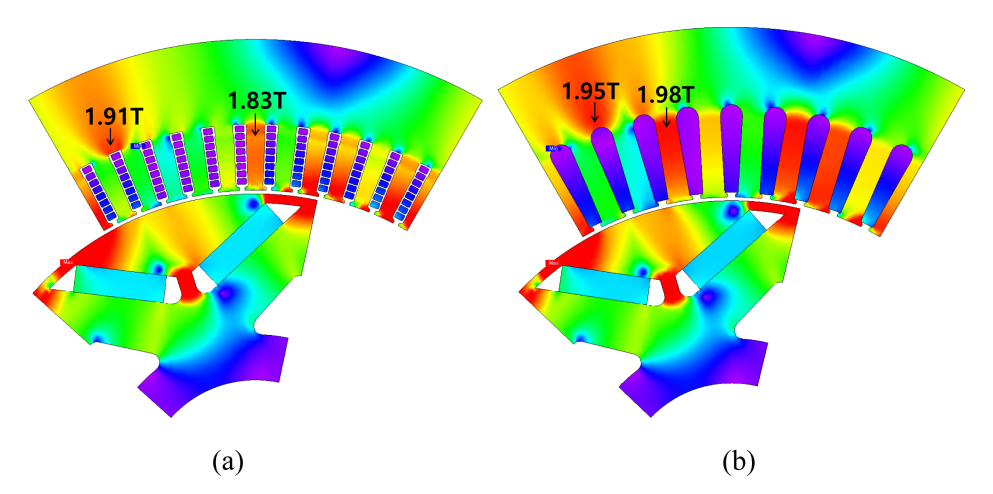


Fig. 4. (Color online) Magnetic Flux Density distribution at Maximum output driving point (a) Hairpin Model, (b) Round Wire Model.

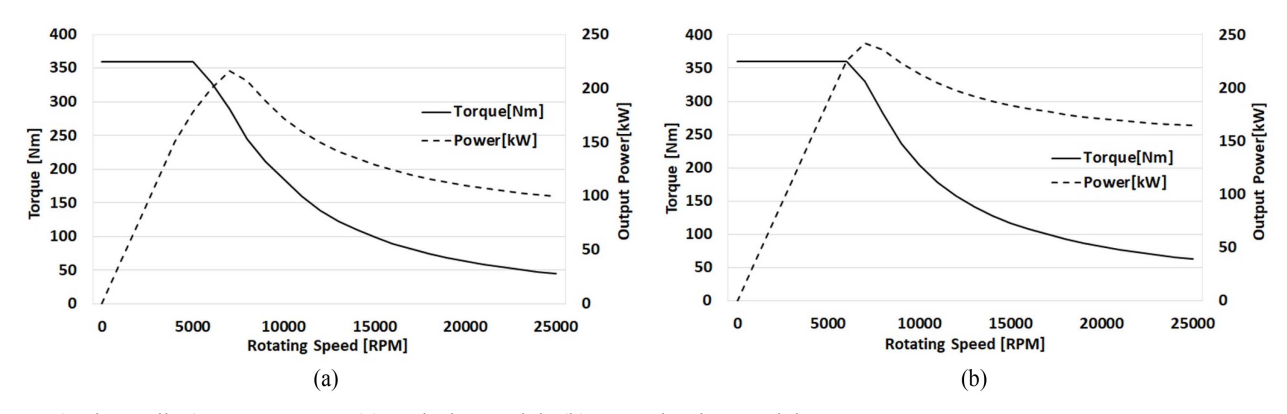


Fig. 5. (Color online) N-T-P Curve (a) Hairpin Model, (b) Round Wire Model.

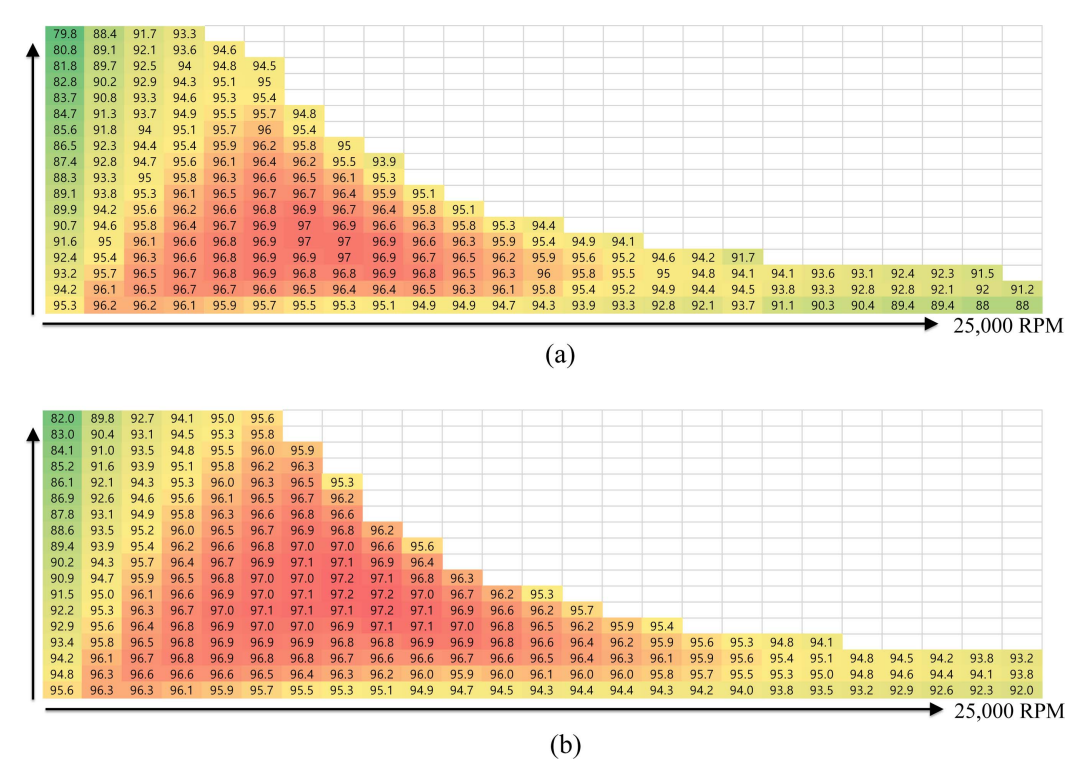


Fig. 6. (Color online) Efficiency Map (a) Hairpin Model, (b) Round Wire Model.

area is required to satisfy the same electric loading because of the lower slot fill factor, resulting in narrower stator teeth, higher magnetic saturation, and increased core loss. As shown in Figs. 5 and 6, the circular wire winding produces no AC copper losses, resulting in higher output and efficiency in the high-speed range.

4. Mechanical Analysis and Prototype Testing Evaluation

4.1. Rotor Stress Reduction Design

If the stress generated in the rotor by the centrifugal force during high-speed rotation exceeds the yield strength of the material, permanent deformation and destruction of the material may occur. Therefore, mechanical safety was improved by designing a structure that reduced the rotor stress and prevented magnet scattering. The material of the rotor core was POSCO's non-oriented electrical steel plate '27PNX1350F,' and the yield strength was 432 [N/mm²]. The main points where the stress was concentrated were set as variables, as summarized in Fig. 7. The shape and maximum stress analysis results for each variable are shown in Fig. 8.

The final rotor shape and stress distribution are shown in Fig. 9. The maximum stress was 399.3 [Mpa] and the safety factor was 1.05.

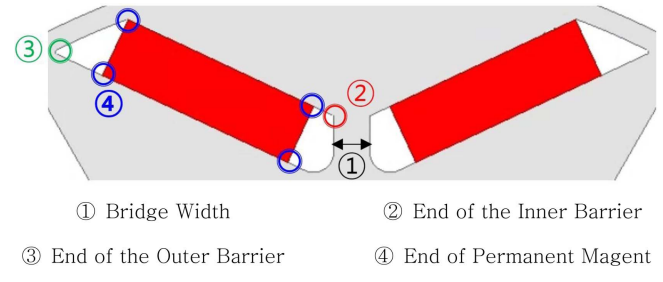


Fig. 7. (Color online) Design Variables for reducing rotor stress.

4.2. Performance Evaluation Tests of the Prototype

To verify the validity of this design, a prototype motor was manufactured using a stator with a round wire and a rotor with a stress-reduction design. A photograph of the active parts of the prototype is shown in Fig. 10. Fig. 11 shows a photograph of the dynamometer test environment for evaluating the output performance of the motor.

To evaluate the performance of the prototype motor under various operating conditions, a dedicated inverter was developed. This inverter is designed to support high-speed, high-current operation, which is essential for accurately verifying the motor's capabilities. In particular, silicon carbide (SiC) MOSFET modules were adopted and connected in a two-parallel configuration to ensure

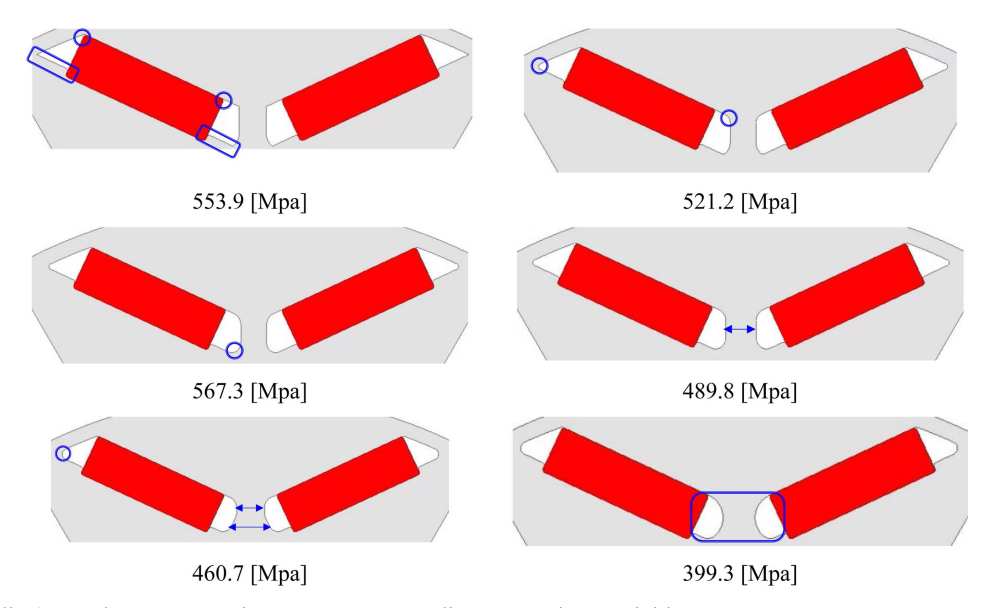


Fig. 8. (Color online) Maximum Stress in rotor core according to Design Variables.

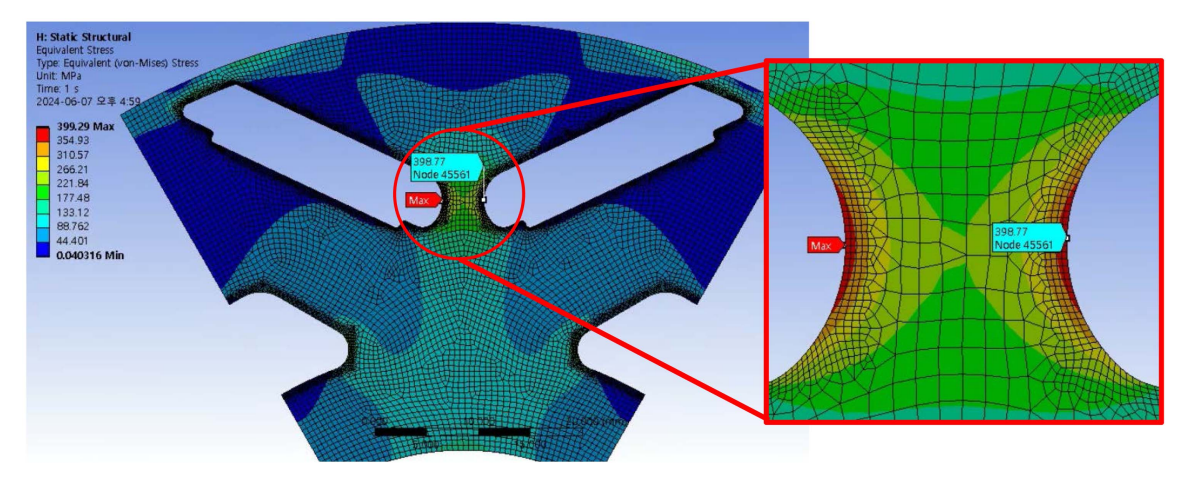


Fig. 9. (Color online) Shape of Final design rotor core.

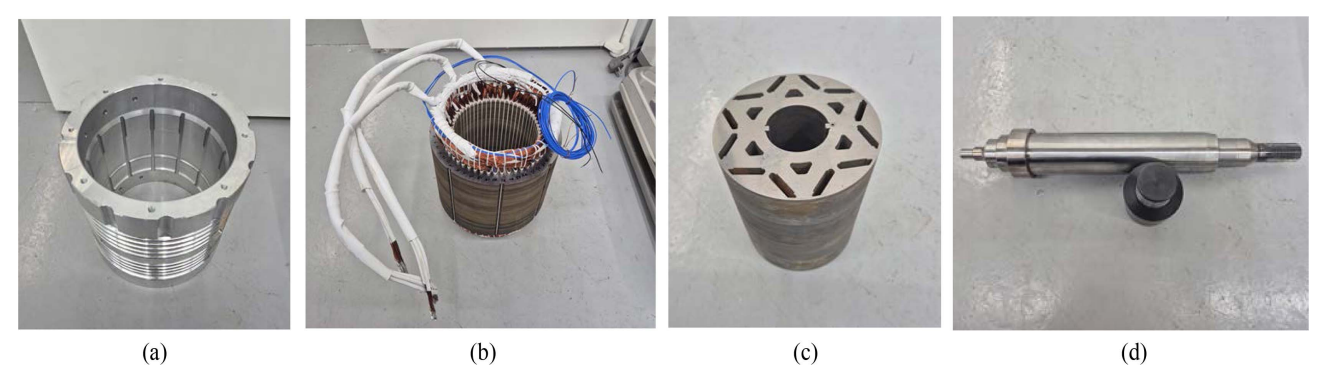


Fig. 10. (Color online) Active Parts of Prototype (a) Housing, (b) Stator, (c) Rotor, (d) Shaft.

high efficiency and fast switching performance.

The inverter operates at a switching frequency of 16[kHz] using space vector pulse width modulation

(SVPWM) and can deliver a maximum output power of 240[kW] with an output current capacity of up to $450[A_{rms}]$. To enable precise control at high rotational

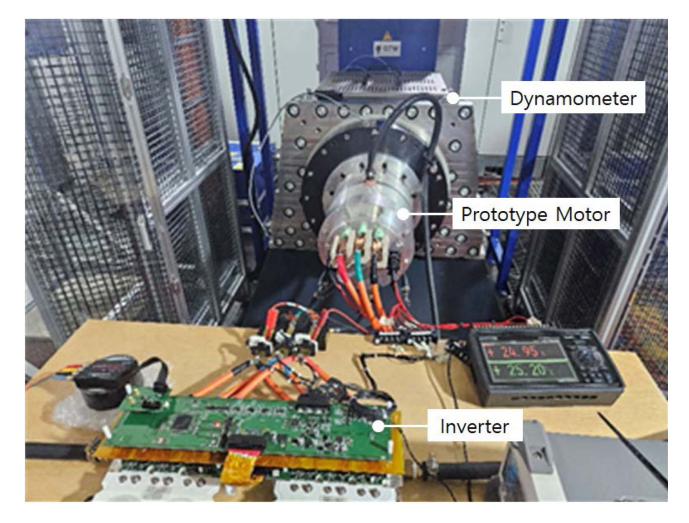


Fig. 11. (Color online) Prototype drive test environment.

speeds, a resolver with an electrical resolution of 10 bits per electrical cycle was employed for rotor position feedback.

The inverter was powered by a DC voltage source ranging from $420[V_{dc}]$ to $820[V_{dc}]$ and cooled using a water-cooling system with a maximum flow rate of 20[L/min]. The specifications of the inverter are summarized in Table 5, and a photograph of the developed inverter is presented in Fig. 12.

4.2.1. Motor Maximum Speed

The dynamo drive program screen and oscilloscope screen at the maximum speed operating point using the dynamometer evaluation equipment of the prototype are shown in Fig. 13. It was confirmed that driving at 21,000[RPM] was possible within an input voltage of $800[V_{dc}]$.



Fig. 12. (Color online) Inverter for prototype motor validation.

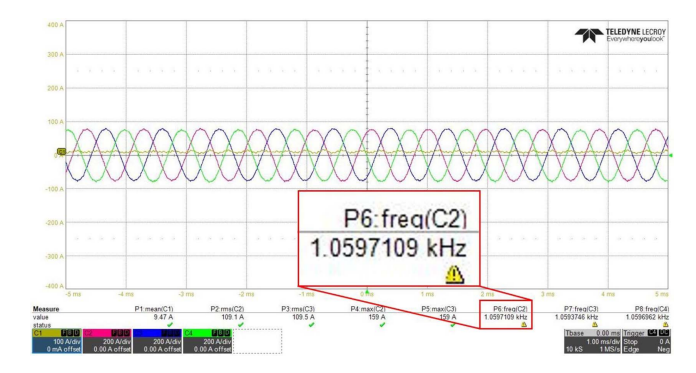


Fig. 13. (Color online) Maximum speed driving point test data.

4.2.2. Motor Maximum efficiency

The power analyzer logging data and oscilloscope screen at the maximum efficiency operating point are shown in Fig. 14. At the operating point of 6,000 [RPM]@270[Nm], the motor output was measured at 169.56[kW], the motor input was measured at 177.15 [kW], and the efficiency was measured at 95.71[%].

Table 5. Specifications of the Inverter for Motor Verification.

Item	Unit	Value	Remark
Power Device	-	SiC MOSFET Module	2-parallel
DC Link Voltage	V_{dc}	420~820	$650V_{nom}$
Input Capacitance	μF	270	2-parallel
Max. Output Power	kW	240	
Max. Output Current	A_{rms}	450	
Max. Efficiency	%	96.0	
Switching Frequency	Hz	16,000	Space Vector PWM
Resolver Electrical Resolution	bit	10	per electrical cycle
LV Supply Voltage	V_{dc}	8~16	$12V_{nom}$
Cooling Water Flow Rate	L/min	Up to 20	

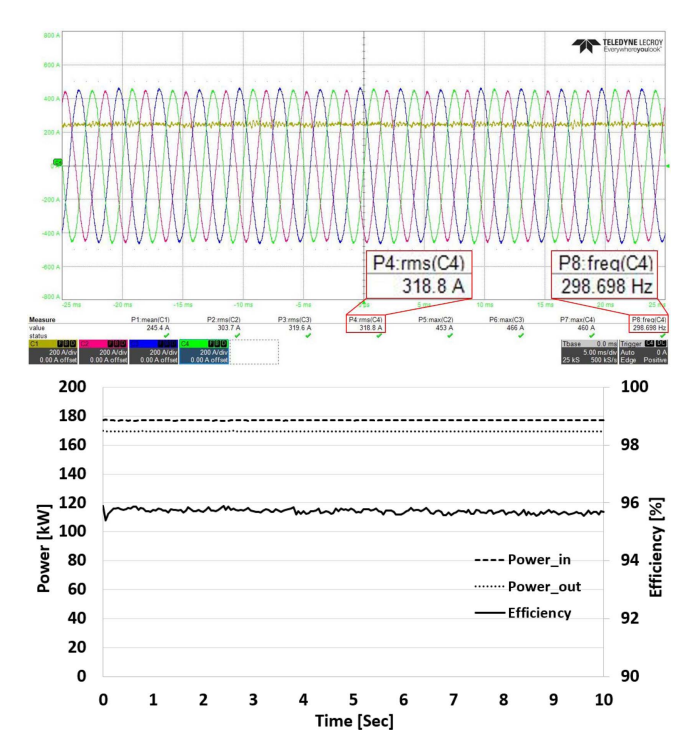


Fig. 14. (Color online) 6000RPM-270Nm driving point Efficiency test data.

5. Conclusion

In this study, we reverse-engineered a commercial 21,000 RPM electric vehicle motor from a leading manufacturer, analyzed its input/output characteristics, and explored electromagnetic and mechanical strategies for improving the motor design to enable operation at a maximum speed of 25,000 RPM. The commercial model analyzed was an interior permanent magnet synchronous motor (IPMSM) with an 8-pole, 48-slot hairpin winding configuration, capable of delivering a maximum output of 220[kW] and operating at up to 21,000 RPM.

To increase the motor's maximum rotational speed, the number of poles was reduced to six to ensure sufficient control resolution within the switching frequency limits of the controller. Two winding configurations were designed for comparison: a hairpin winding model and a round-wire model using parallel strands. The hairpin model demonstrated high power density due to its high slot-fill factor; however, as the rotational speed increased, AC losses in the winding rose significantly, resulting in reduced output and efficiency in the high-speed range. In contrast, the round-wire model exhibited a lower slot-fill

factor and higher magnetic saturation relative to the core volume, leading to increased iron losses. Nevertheless, because AC loss does not occur in the winding, the model showed relatively higher output and efficiency at high speeds. Owing to its favorable manufacturability, lower production cost, and superior high-speed performance, the round-wire model was selected as the prototype. Its mechanical stability was ensured through a rotor design that minimized stress under high-speed operation.

Finally, the validity of the proposed design and analysis was verified through prototype testing, including assessments of maximum speed, maximum efficiency, and power density.

Acknowledgment

This work was supported by the Korea Institute of Energy Technology Evaluation and Planning (KETEP) grant funded by the Korea government (MOTIE) (RS-2024-00419152).

References

- [1] Y.-H. Jung, M.-R. Park, K.-O. Kim, J.-W. Chin, J.-P. Hong, and M.-S. Lim, IEEE Trans. Ind. Appl. 57, 327 (2021).
- [2] T. Zou, D. Gerada, A. L. Rocca, M. Moslemin, A. Cairns, M. Cui, A. Bardalai, F. Zhang, and C. Gerada, IEEE Transactions on Transportation Electrification 8, 3578 (2022).
- [3] J. Nerg, M. Rilla, V. Ruuskanen, J. Pyrhönen, and S. Ruotsalainen, IEEE Trans. Ind. Electron. 61, 4286 (2014).
- [4] X. Ju, Y. Cheng, M. Yang, S. Cui, A. Sun, X. Liu, and M. He, IEEE Trans. Ind. Electron. **69**, 8803 (2022).
- [5] S. M. Goetz, R. Lizana F., and S. Rivera, Proceedings of the IEEE **112**, 1831 (2024).
- [6] S.-H. Park, J.-W. Chin, K.-S. Cha, J.-Y. Ryu, and M.-S. Lim, IEEE Trans. Ind. Electron. 70, 12102 (2023).
- [7] F. Chai, Y. Li, P. Liang, and Y. Pei, IEEE Trans. Ind. Electron. **63**, 3420 (2016).
- [8] G. Chu, R. Dutta, M. F. Rahman, H. Lovatt, and B. Sarlioglu, IEEE Trans. Ind. Appl. **56**, 1321 (2020).
- [9] I. Husain, B. Ozpineci, M. S. Islam, E. Gurpinar, G. J. Su, W. Yu, S. Chowdhury, and L. Xue, Proceedings of the IEEE 109, 1039 (2021).
- [10] D. Fodorean, IEEE Trans. Magn. 50, 921 (2014).
- [11] Y. Yang, S. M. Castano, R. Yang, M. Kasprzak, B. Bilgin, A. Sathyan, H. Dadkhah, and A. Emadi, IEEE Transactions on Transportation Electrification 3, 86 (2017).